Preparation of Ti incorporated Y zeolites by a post-synthesis method under acidic conditions and their catalytic properties

Yasunori Oumi[a,*], Takuya Manabe[b], Hitoshi Sasaki[b], Toshiyasu Inuzuka[a], Tsuneji Sano[b,**]

[a]Division of Instrument Analysis, Life Science Research Center, Gifu University, Yanagito 1-1, Gifu 501-1193, Japan

[b]Department of Applied Chemistry, Graduate School of Engineering, Hiroshima University, Kagamiyama 1-4-1, Higashi-Hiroshima 739-8527, Japan

*Corresponding author

Tel. : +81-58-293-2037, Fax: +81-58-293-2036, E-mail: oumi@gifu-u.ac.jp (Y. Oumi),

**Corresponding author

Tel. : +81-82-424-7607, Fax: +81-82-424-5494, E-mail: tsano@hiroshima-u.ac.jp (T. Sano)

Abstract

Ti incorporated Y zeolites were prepared by post-synthesis treatment of a dealuminated USY zeolite with an aqueous solution of $(NH_4)_2TiF_6$, and characterized by XRD, ^{27}Al MAS NMR, FT-IR, SEM, TEM, UV-vis, and XANES techniques. The results showed that Ti species were tetrahedrally incorporated into the hydroxyl nests in the zeolite framework under acidic conditions. Furthermore, the catalytic performance of Ti incorporated Y zeolites in epoxidation of cycloalkenes using an aqueous solution of hydrogen peroxide was higher than that of TS-1 zeolite.

Keywords: Ti incorporated Y zeolite, Post-synthesis, Dealumination, Titanation, Epoxidation

1. Introduction

Generally, the physicochemical properties of zeolites depend on the number of tetrahedrally coordinated Al atoms in the zeolite framework. In order to improve the physicochemical properties of zeolites, therefore, isomorphous substitution of framework Al by various metals such as Ga, Fe, B, V, Zn, and Ti has been widely studied [1-3]. Isomorphous substitution is achieved by direct hydrothermal synthesis or by post-synthesis treatment. The post-synthesis replacement of tetrahedrally coordinated framework Al by heteroatoms is a suitable method if direct synthesis of the materials fails or if synthesis is difficult to achieve. Since the first report of direct synthesis of a Ti incorporated zeolite (titanosilicate), TS-1 with an MFI-type structure, by Taramasso et al. in 1983, there have been many investigations into synthesis, characterization, and catalytic applications of titanosilicates. TS-1 zeolites with a 10-membered ring (10 -MR) pore system exhibit unique catalytic activity for epoxidation of alkenes and for oxidation of alkanes and alcohols under mild reaction conditions using an aqueous solution of hydrogen peroxide as the oxidant [4-6]. However, the catalytic activity of TS-1 zeolites is low when bulky substrates such as cyclic or branched molecules are used as reagents. Therefore, the preparation of titanosilicates with a larger pore system has received a lot of attention. Incorporation of Ti into zeolites with a large pore system (12-MR), such as Y zeolite, β zeolite, and mordenite, has been investigated by many research groups. As it is not so easy to synthesize Ti incorporated zeolites by direct hydrothermal synthesis, several post-synthesis treatments such as ion-exchange [9], impregnation, and treatment with $TiCl_4$ and $(NH_4)TiF_6$ [10-15] have been proposed. However, the formation of non-framework Ti species has been observed.

Recently, we have investigated the reversibility of the dealumination-realumination process for several zeolites such as mordenite, ZSM-5 and β zeolites; we also studied metal incorporation into zeolites by a post-synthesis method involving adjustment of the pH values of aqueous solutions containing metal sources under acidic conditions [16-19]. Ga and Al species in solution were easily reinserted into the β framework under acidic conditions [20]. We also found that some of the non-framework Al species in dealuminated Y zeolites could be effectively reinserted into the zeolite framework [21]. These results

strongly suggest the possibility of inserting Ti into the zeolite framework.

In this research, we investigated the incorporation of Ti into Y zeolites under acidic conditions by a post-synthesis method, and their catalytic performances were evaluated using epoxidation of cycloalkenes as a test reaction.

2. Experimental

2.1. Dealumination and titanation of Y zeolites

A Na-type Y zeolite (NaY, $Si/Al_2 = 5$, JGC Catalysts and Chemicals Ltd. Co., Japan) was used as the parent zeolite. The ammonium cation exchanged Y zeolite (NH_4Y) was prepared by a conventional ion-exchange method using an aqueous solution of 1 M $(NH_4)_2SO_4$, and was calcined at 400 ºC, yielding the protonated Y zeolite (HY). Ion-exchange of the HY zeolite was again performed using a 1 M $(NH_4)_2SO_4$ aqueous solution, followed by steaming at 700 ºC, yielding a ultra-sable Y zeolite (USY-5). In the term USY-XX, XX denotes the bulk Si/Al_2 molar ratio. USY-50 zeolite was prepared by NH_4^+ ion-exchange, steaming, and dealumination of the USY-5 zeolite. Dealumination of the USY-5 zeolite was carried out by stirring the zeolite in an aqueous 25 wt% sulfuric acid solution at 75 ºC for 1 h. The sample was then filtered, washed thoroughly with hot deionized water (60 ºC), and dried at 120 ºC. Incorporation of Ti into the USY-50 zeolite was carried out by a post-synthesis method under acidic conditions. The dealuminated USY-50 zeolite(1g) was added to $(NH_4)_2TiF_6$ (Aldrich) solutions(100 ml) with different concentrations (1 – 10 mM). To control of the pH value of the suspension during titanation, we added a certain amount of a 25 wt% sulfuric acid aqueous solution (pH = 1 and 3) or a 25 wt% ammonium aqueous solution (pH = 5) to the suspension. The mixtures were stirred at room temperature for 24 h and the samples were filtered, washed thoroughly with hot deionized water (60 ºC) and dried at 120 ºC. The samples were then calcined at 500 ºC for 10 h, to give Ti-USY-50-YY, where YY denotes the concentration of the $(NH_4)_2TiF_6$ aqueous solution. The zeolites obtained are summarized in Table 1.

2.2. Characterization

Identification of the zeolites obtained was achieved by X-ray diffraction (XRD; Bruker X D8 ADVANCE) using Cu Kα radiation. The bulk chemical composition was measured by X-ray fluorescence (XRF; Philips PW2400). Samples were prepared by the glass bead method (THG-6, Tosoku Laboratory, Japan). Textural properties were determined by N_2 adsorption (Bel Japan Belsorp 28SA, Bel Japan, Inc., Japan). Before the adsorption measurements, which were carried out at –196 ºC, the powdered samples (ca. 0.1 g) were evacuated at 400 ºC for 10 h. The IR spectra were recorded on a FT-IR spectrometer (JEOL JIR-7000, JEOL, Japan) at a resolution of 4 cm^{-1} and an accumulated number of 500 at room temperature. The samples were prepared as self-supporting thin wafers, and placed in a quartz IR cell with CaF_2 windows. Prior to the measurements, each sample was dehydrated under vacuum at 400 ºC for 3 h. For IR spectra in the framework vibration region, the KBr technique was used. Samples were mixed with KBr (KBr/zeolite = 99/1 wt%). Prior to the measurements, each sample was dehydrated under vacuum at 150 ºC for 3 h. UV-vis diffuse reflectance spectra of the zeolites were recorded on a UV-vis spectrometer (JASCO V-570, Jasco, Japan) with a bandwidth of 10 mm and a scan speed of 400 nm/min. The XANES spectra in the energy range 4950-5030 eV were measured at room temperature on the HiSOR beam line BL-11 with a Si(111) monochromator at Hiroshima University. The step size and the counting time were 0.5 eV/step and 5.0 s, respectively. High-resolution transmission electron microscope (TEM) images were obtained using a JEOL JEM-2100 microscope (JEOL, Tokyo, Japan) with an accelerating voltage of 200 kV.

2.3. Catalytic tests

Epoxidation reactions of cyclohexene, cyclooctene, and cyclododecene (Wako Pure Chemical Ind. Ltd., Japan) were carried out in a glass reactor at 50 ºC for 5 h with vigorous stirring. Acetonitrile (Tokyo Chemical Ind. Co. Ltd., Japan) and tetrahydrofuran (Wako Pure Chemical Ind. Ltd., Japan) were used as solvents; acetonitrile for cyclohexene and cyclooctene, and tetrahydrofuran for cyclododecene. Each reaction was carried out using 50 mg of catalyst dehydrated under vacuum at 400 ºC, 10 ml of solvent, 10

mmol of substrate, and 0.2 ml of an aqueous solution of 30 wt % hydrogen peroxide (Wako Pure Chemical Ind. Ltd., Japan). After a certain reaction time, the reaction solutions were filtered using a membrane filter. The solutions were then analyzed on a gas chromatograph (GC; GC-17A , Shimadzu, Japan) equipped with a 60 m capillary column (ZB-1, Phenomenex Inc., USA) and a flame ionization detector. 1-Hexanol (Wako Pure Chemical Ind. Ltd., Japan) was used as an internal standard for all reactions.

3. Results and discussion

3.1. Dealumination of Y zeolites

Figures 1(a and b) show the XRD patterns of the parent NaY and the dealuminated USY-50 zeolites. In the USY-50 zeolite XRD pattern, there were no peaks other than those corresponding to FAU-type structures. However, a slight shift in the peak positions was observed. This shift is due to lattice shrinkage as a result of dealumination [21, 22]. The characteristics of the parent NaY and the dealuminated USY-50 zeolites are listed in Table 1. Although the bulk Si/Al_2 ratios obtained by XRF increased from 5 to 50 after the dealumination treatment, the USY-50 zeolite micropore volume was the same as that of the parent NaY zeolite, indicating that the zeolite framework structure was maintained even after the dealumination process. However, a considerable increase in the mesopore volume was observed, suggesting mesopore formation [23, 24]. As shown in Fig. 2 (a and b), no change in the morphology was observed between NaY and USY-50 zeolites.

To get a better understanding of the dealumination process, we measured ^{27}Al MQ MAS NMR and FT-IR spectra. Figure 3 shows the ^{27}Al MQ MAS NMR spectra of various Y zeolites. The NaY zeolite spectrum shows only one peak, at ca. 60 ppm, assigned to an Al^{IV} site (Fig. 3 (a)), which is in agreement with the fact that X-ray structural analysis showed only one crystallographically independent tetrahedral site in the NaY zeolite. However, the spectrum of the USY-5 zeolite ($Si/Al_2 = 5$) had two peaks at ca. 40 and 0 ppm, as well as the peak at ca. 60 ppm; these peaks were assigned to Al^{V} and Al^{VI} species [25], respectively (Fig. 3 (b)). This indicates generation of non-framework Al species as a result of the steaming

treatment [26]. The presence of non-framework Al species in the USY-5 zeolite was also confirmed by reductions in the micropore surface area and volume (Table 1). After H_2SO_4 treatment of the USY-5 zeolite, the peaks resulting from non-framework Al species disappeared completely, as can be seen in the spectrum of the dealuminated USY-50 zeolite (Fig. 3 (c)). The FT-IR spectra of the HY and USY-50 zeolites in the 4000-3000 cm^{-1} region are shown in Fig. 4. The peaks at ca. 3550 cm^{-1} and 3630 cm^{-1} in the HY zeolite spectrum were assigned to acidic bridging OH groups of Si(OH)Al in α- and β-cages, respectively, in Y zeolite [27]. After dealumination, the intensities of the peaks at ca. 3550 cm^{-1} and 3630 cm^{-1} decreased markedly in the USY-50 zeolite spectrum. Clear increases in the intensities at ca. 3500 cm^{-1} and 3745 cm^{-1}, assigned to hydrogen-bonded silanol groups (hydroxyl nests) and isolated silanol groups, respectively, were observed.

3.2. Ti incorporation into Y zeolites

Post-synthesis titanation was performed in the liquid phase. $(NH_4)_2TiF_6$ was employed as a Ti source. The molecular size of TiF_6 anion was estimated to be ca. 6.2 Å by DFT quantum chemical calculation (DMol3 Ver. 5.0 provided by Accelrys, Inc.), which allowed the diffusion of TiF_6 anion into the supercages (ca. 7.4 Å) of Y zeolite. In the previous work [21], we found that the amount of incorporated Al increased with an increase in the pH value of the suspension during realumination. Therefore, at first titanation was carried out using a 2 mM $(NH_4)_2TiF_6$ solution at various pH values (1, 3 and 5). Figure 1 (c) shows the XRD pattern of the titanated USY-50 zeolite prepared (Ti-USY-50-2, sample no. 4). There were no peaks other than those corresponding to FAU-type structures. Only slight decreases in the peak intensities were observed. The yield of Ti incorporated Y zeolite was 65 - 74 % based on the weight of USY-50. The bulk Si/Ti ratio slightly decreased with an increase of pH value (Table 1). The bulk Si/Al_2 ratio was considerably larger than that of USY-50 zeolite, indicating that dealumination occurred during titanation process. This was also confirmed from the ^{27}Al MQ MAS NMR spectrum (Fig. 3 (d)). Figures 5 (a, b and c) show the UV-vis spectra of Ti-USY-50-2 (sample no.4), Ti-USY-50-2-pH3 (sample no.5), and Ti-USY-50-2-pH5 (sample no.6) zeolites. In the spectrum of Ti-USY-50–2 zeolite prepared at pH 1, the

peak from four-coordinated Ti species was observed at ca. 220 nm [28]. On the other hand, in the spectra of Ti-USY-50-2-pH3 and Ti-USY-50-2-pH5 zeolites, shoulder peaks assigned to six-coordinated species and to TiO_2 (anatase) were observed at ca. 280 nm and 330 nm, respectively, suggesting that the pH value is a crucial factor for incorporation of Ti atoms into the framework of FAU-type zeolites. Figure 6 shows the FT-IR spectra of USY-50 and Ti-USY-50-2 zeolites in the 1600-400 cm^{-1} region. The Ti-USY-50-2 spectrum had a peak at ca. 960 cm^{-1}. This peak can be assigned to the stretching vibration of four-coordinated Ti species in the zeolite framework [29, 30]. As the Ti-USY-50 zeolite prepared at pH 1 had the highest Si/Al_2 ratio i.e. the smallest Al content, the pH value of suspension during titanation treatment was fixed at 1 in the following experiments.

Next, the USY-50 zeolite was suspended in $(NH_4)_2TiF_6$ aqueous solutions of different concentrations(1, 2, 3, 5, and 10 mM) at pH 1. As described previously, in the Ti-USY-50-2 zeolite XRD pattern, there were no peaks other than those corresponding to FAU-type structures. However, the peak intensities in the XRD pattern of Ti-USY-50-3 zeolite (sample no. 8) prepared from a 3 mM $(NH_4)_2TiF_6$ aqueous solution decreased markedly, indicating structural degradation (Fig. 1 (d)). The characteristics of various Ti-USY-50 zeolites are listed in Table 1. N_2 adsorption measurements showed that the micropore surface area and volume of Ti-USY-50-2 zeolite were the same as those of the parent NaY zeolite. However, the micropore surface area decreased monotonously with increasing $(NH_4)_2TiF_6$ aqueous solution concentration, while the external surface area and the mesopore volume increased. The bulk Si/Al_2 ratio also increased with increasing the $(NH_4)_2TiF_6$ aqueous solution concentration. This also strongly indicated that dealumination occurred during titanation of the USY-50 zeolite. Figures 2 (c and d) show SEM images of the Ti-USY-50 zeolites. The Ti-USY-50-2 crystals were almost the same as the USY-50 crystals. However, the SEM image of Ti-USY-50-10 zeolite prepared from a 10 mM $(NH_4)_2TiF_6$ solution (sample no. 10) shows that partial degradation of the crystals occurred, and amorphous materials were observed (Fig. 2 (d)).

To obtain further evidence that Ti atoms are incorporated into the zeolite framework as four-coordinated Ti species, we measured the XANES spectra. Figure 7 shows the XANES spectra of Ti-USY-50-2, and of TiO_2 (anatase) as a reference. In the Ti-USY-50-2 zeolite spectrum, a sharp pre-edge

peak was clearly observed at 4967 eV, indicating generation of four-coordinated Ti species [31]. The peak assigned to TiO_2 (anatase) was not observed in the spectrum. The Ti-USY-5 zeolites were also characterized by TEM-EDX (Fig. 8). No TiO_2 particles were observed. However, mesopore formation was confirmed, which was consistent with an increase in mesopore volume (Table 1). In addition, the surface Si/Ti molar ratios measured by EDX depended on the number of analytical points (30~170), strongly indicating that titanation did not proceed uniformly. This is probably attributable to heterogeneous distribution of the hydroxyl nests generated during dealumination.

From the above results, one may conclude that Ti species in solution are incorporated into the Y zeolite frameworks as four-coordinated Ti species.

3.3. Epoxidation of cycloalkenes

To clarify the catalytic performance of the Ti-USY-50 zeolites obtained, we carried out the epoxidation of cyclohexene, cyclooctene, and cyclododecene. For comparison, TS-1 zeolite supplied by Japan Reference Catalyst, the Catalysis Society of Japan was also used. The results are summarized in Table 2. Although cycloalkene epoxidation occurred with these zeolites, large differences in the conversion rates and epoxide selectivities were observed between Ti-USY-50 and TS-1 zeolites. Especially, in the case of cyclohexene epoxidation, the Ti-USY-50 zeolite gave higher conversion rates and epoxide selectivities than the TS-1 zeolite, which is known to be an effective epoxidation catalyst. The cyclohexene conversion on Ti-USY-50-2 zeolite was slightly larger than that on Ti-USY-50-1 zeolite because of slightly higher Ti content. However, little difference in epoxide selectivity was observed. The lower cyclohexene conversion and epoxide selectivity on Ti-USY-50-3 and Ti-USY-50-5 zeolites are probably due to partial degradation of zeolite framework structure. For both Ti-USY-50-2 and TS-1 zeolites, the cycloalkene conversion rates decreased in the following order: cyclohexene > cyclooctene > cyclododecene. Given that the Y zeolite pore size (12-MR, ca. 7.4Å) is larger than that of TS-1 (10-MR, ca. 5.4 Å), and that the molecular diameters of cyclohexene, cyclooctene, and cyclododecene are 5.0 Å, 5.7 Å, and 7.6 Å, respectively, it is not easy for cyclododecene molecules to enter the supercages of Y zeolite. Namely, the lower conversion of

cyclododecene means that the epoxidation reactions take place in zeolitic pores [32].

4. Conclusions

The results showed that Ti species in solution were incorporated into hydroxyl nests in the zeolite framework. These nests were generated during dealumination. The incorporated Ti species were tetrahedral. Furthermore, the catalytic performance of Ti incorporated Y zeolites in epoxidation of cycloalkenes using aqueous hydrogen peroxide was higher than that of TS-1 zeolite.

Acknowledgements

The authors thank Professor Shinjiro Hayakawa at Hiroshima University for XANES measurements.

References

[1] M. Tamura, W. Chaikittisilp, T. Yokoi, T. Okubo, Micropor. Mesopor. Mater. 112 (2008) 202 - 210.

[2] Q.-H. Xia, T. Tatsumi, Mater. Chem. Phys. 89 (2005) 89 - 98.

[3] V. R. Choudhary, S. K. Jana, Appl. Catal. A:Gen. 224 (2002) 51 - 62.

[4] E. Spanó, G. Tabacchi, A. Gamba, E. Fois, J. Phys. Chem. B 110 (2006) 21651 - 21661.

[5] J. Limtrakul, C. Inntam, T. N Truong, J. Mol. Catal. A:Chem. 207 (2004) 139 - 148.

[6] Q. -H. Xia, X. Chen, T. Tatsumi, J. Mol. Catal. A:Chem. 176 (2001) 179 - 193.

[7] S.-H. Chien, Y.-K. Tseng, M.-C. Lin, J.-C. Ho, Stud. Surf. Sci. Catal. 98 (1995) 7 - 8.

[8] G. Grubert, M. Wark, N. I. Jaeger, G. Schulz-Ekloff, J. Phys. Chem. B 102 (1998) 1665 - 1671.

[9] S. Anandan, M. Yoon, J. Photochem. Photobiol. C 4 (2003) 5 - 18.

[10] Z. Tvaruozˇkova´, N. Zˇilkova´, Appl. Catal. A:Gen. 103 (1993) L1 – L4.

[11] Y. Wang, A. Zhang, Q. Xu, R. Chen, Appl. Catal. A:Gen. 214 (2001) 167 - 177.

[12] T. Tatsumi, M. Nakamura, S. Negishi, H. Tominaga, J. Chem. Soc. Chem. Commun. (1990) 476 -477.

[13] T. Tatsumi, M. Nakamura, K. Yuasa, H. Tominaga, Catal. Lett. 10 (1991) 259 - 262.

[14] P. Wu, T. Tatsumi, J. Phys. Chem. B 106 (2002) 748 - 753.

[15] G. P. Schindler, P. Bartl, W. F. Hoelderich, Appl. Catal. A:Gen. 166 (1998) 267 - 279.

[16] T. Sano, R. Tadenuma, Z.B. Wang, K. Soga, J. Chem. Soc., Chem. Commun. (1997) 1945 - 1946.

[17] T. Sano, Y. Uno, Z.B. Wang, C.H. Ahn, K. Soga, Micropor. Mesopor. Mater. 31 (1999) 89 - 95.

[18] Y. Oumi, R. Mizuno, K. Azuma, S. Nawata, T. Fukushima, T. Uozumi, T. Sano, Micropor. Mesopor. Mater. 49 (2001) 103 - 109.

[19] Y. Oumi, S. Nemoto, S. Nawata, T. Fukushima, T. Teranishi, T. Sano, Mater. Chem. Phys. 78 (2002) 551 - 557.

[20] Y. Oumi, I. Jintsugawa, S. Kikuchi, S. Nawata, T. Fukushima, T. Teranishi, T. Sano, Micropor. Mesopor. Mater. 66 (2003) 109 - 116.

[21] Y. Oumi, J. Takahashi, K. Takeshima, H. Jon, T Sano, J Porous Mater. 14 (2007) 19 - 26.

[22] B. A. Holmberg, H. Wang, Y. Yan, Micropor. Mesopor. Mater. 74 (2004) 189 - 198.

[23] A. Zukal, V. Patzelová, U. Lohse, Zeolites 6 (1986) 133-136.

[24] A. Gola, B. Rebours, E. Milazzo, J. Lynch, E. Benazzi, S. Lacombe, L. Delevoye, C. Fernandez, Micropor. Mesopor. Mater. 40 (2000) 73 - 83.

[25] Z. Yan, D. Ma, J. Zhuang, X. Liu, X. Liu,X. Han, X. Bao, F. Chang, L. Xu, Z. Liu, J. Mol. Catal. A:Chem. 194 (2003) 153 - 167.

[26] S. Ganapathy, K. U. Gore, R. Kumar, J.-P. Amoureux, Solid State Nucl. Magn. Reson. 24 (2003) 184 - 195.

[27] Y. Li, J. N. Armor, Appl. Catal. A:Gen. 183 (1999) 107 - 120.

[28] A. Carati, C. Flego, E. P. Massara, R. Millini, L. Carluccio, W. O. ParkerJr., G. Bellussi, Micropor. Mesopor. Mater. 30 (1999) 137 - 144.

[29] C. S. Cundy, J. O. Forrest, Micropor. Mesopor. Mater. 72 (2004) 67 - 80.

[30] G. Ricchiardi, A. Damin, S. Bordiga, C. Lamberti, G. Spanò, F. Rivetti, A. Zecchina, J. Am. Chem. Soc. 123 (2001) 11409 - 11419.

[31] V. Bolis, S. Bordiga, C. Lamberti, A. Zecchina, A. Carati, F. Rivetti, G. Spanò, G. Petrini , Micropor. Mesopor. Mater. 30 (1999) 67 - 76.

[32] C. B. Dartt, M. E. Davis, Appl. Catal. A :Gen. 143 (1996) 53 – 73.

Figure captions

Fig. 1 XRD patterns of NaY, USY-50, and Ti-USY-50. Sample nos. (a) 1, (b) 3, (c) 4, and (d) 8.

Fig. 2 SEM images of NaY, USY-50, and Ti-USY-50. Sample nos. (a) 1, (b) 3, (c) 4, and (d) 10.

Fig. 3 ^{27}Al MQMAS NMR spectra of various Y-type zeolites. Sample nos. (a) 1, (b) 2, (c) 3, and (d) 4.

Fig. 4 FT-IR spectra of (a) HY and (b) USY-50.

Fig. 5 UV-vis diffuse reflectance spectra of Ti-USY-50. Sample nos. (a) 4 , (b) 5, and (c) 6.

Fig. 6 FT-IR spectra of (a) USY-50 and (b) Ti-USY-50-2.

Fig. 7 XANES spectra of (a) Ti-USY-50-2 and (b) TiO_2 (anatase).

Fig. 8 TEM image and surface Si/Ti molar ratio of Ti-USY-50-2.

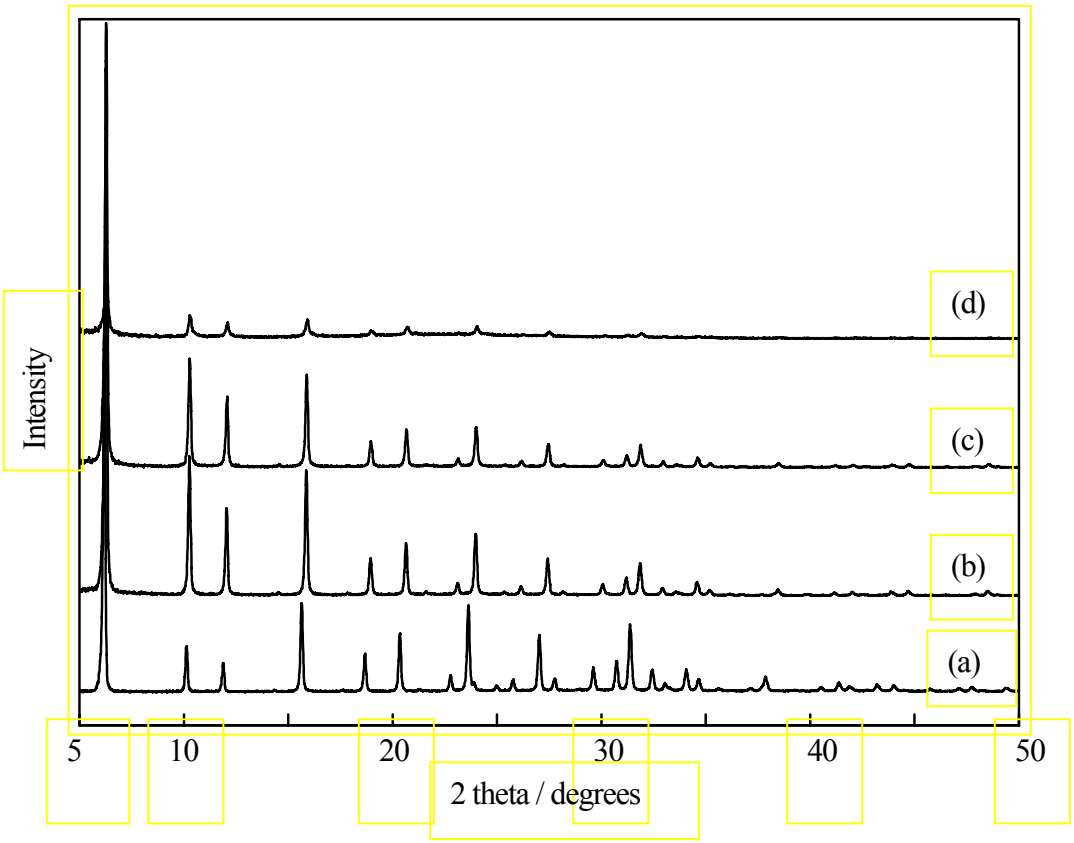

Figure 1. Y. Oumi et al.

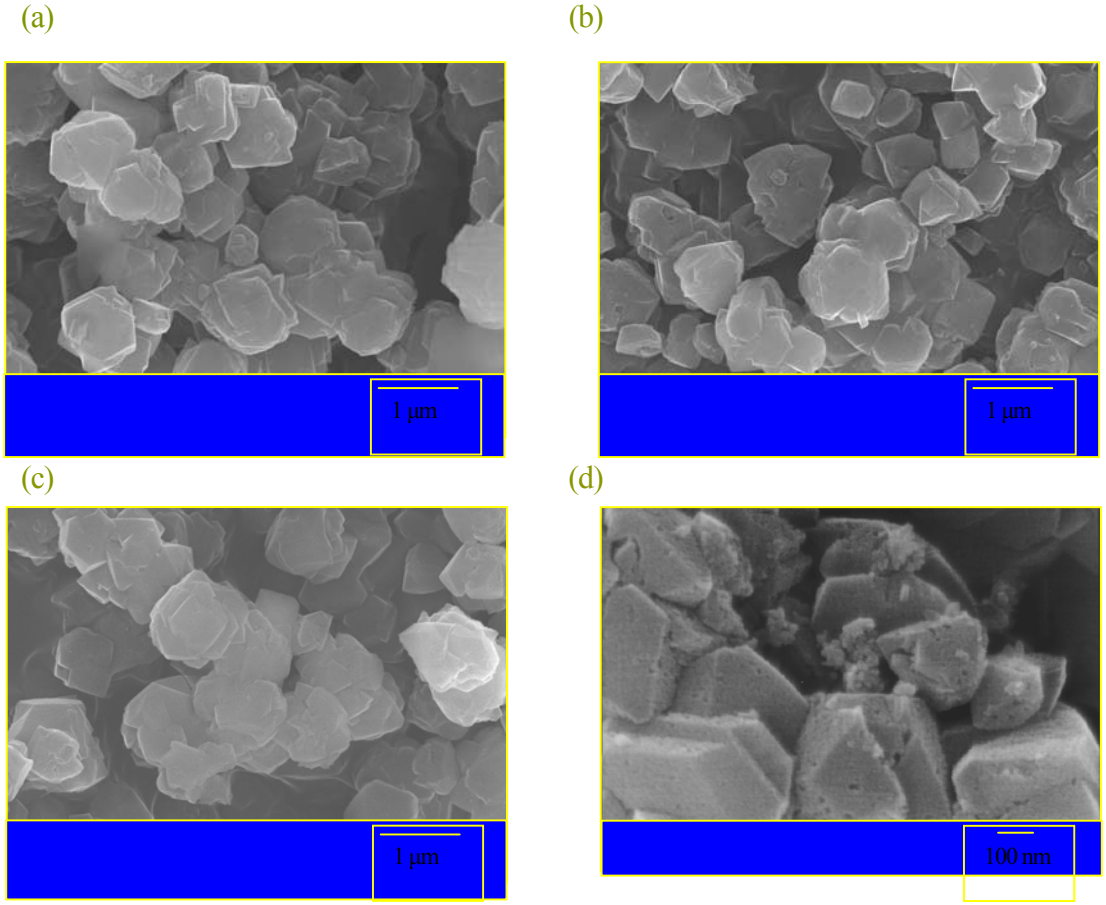

Figure 2. Y. Oumi et al.

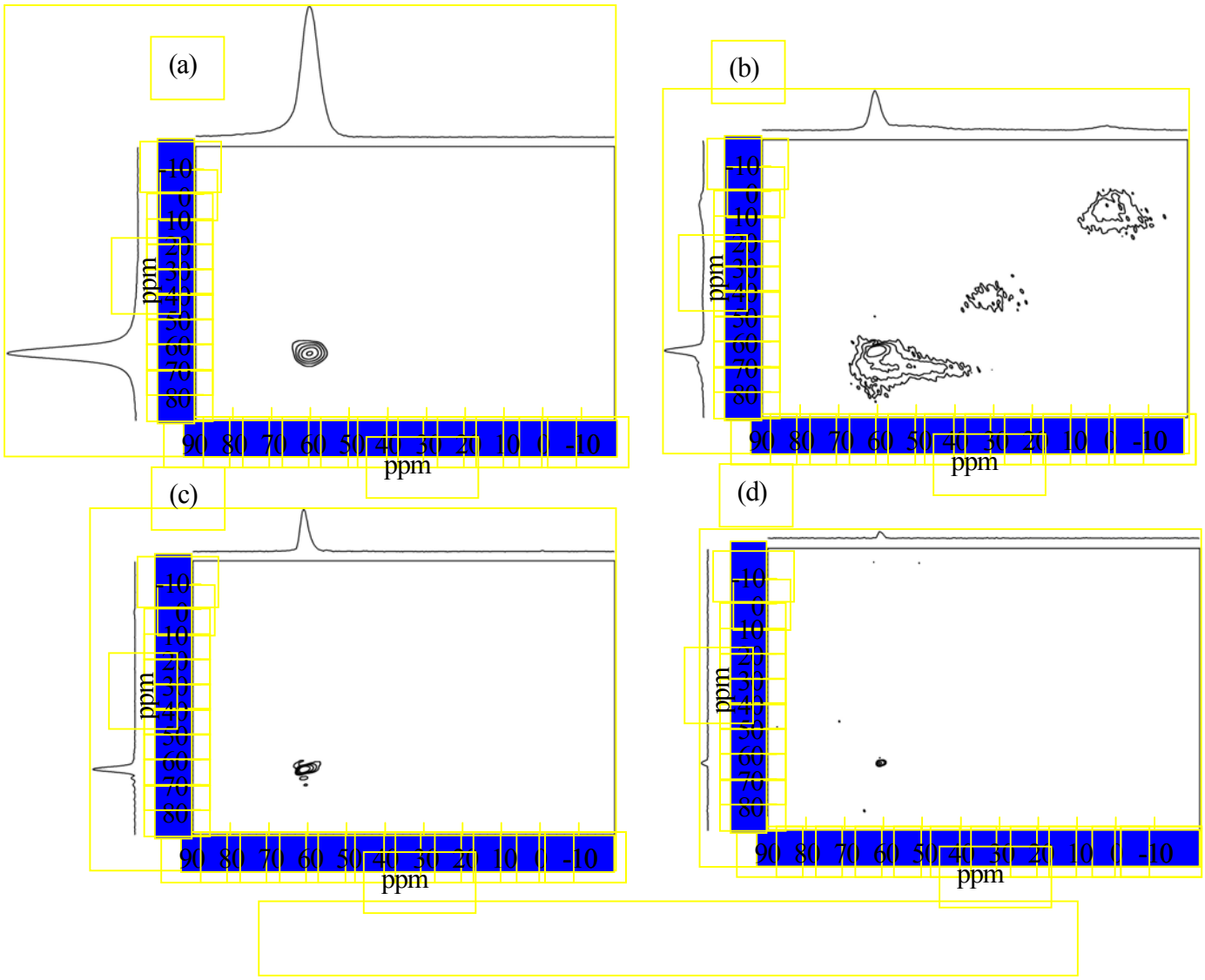

Figure 3. Y. Oumi et al.

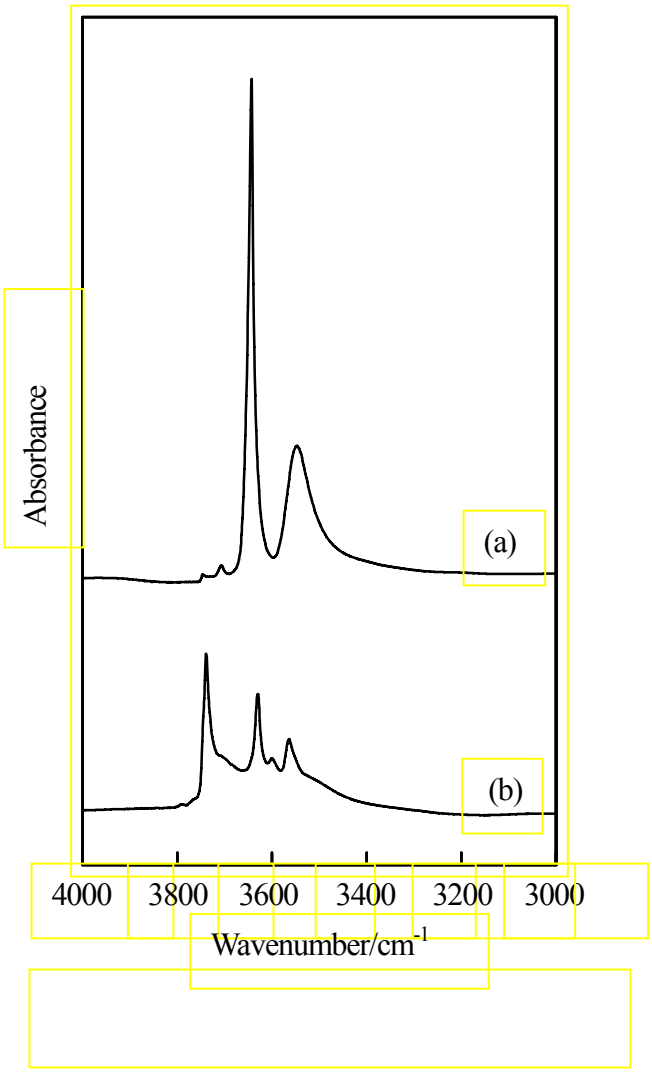

Figure 4. Y. Oumi et al.

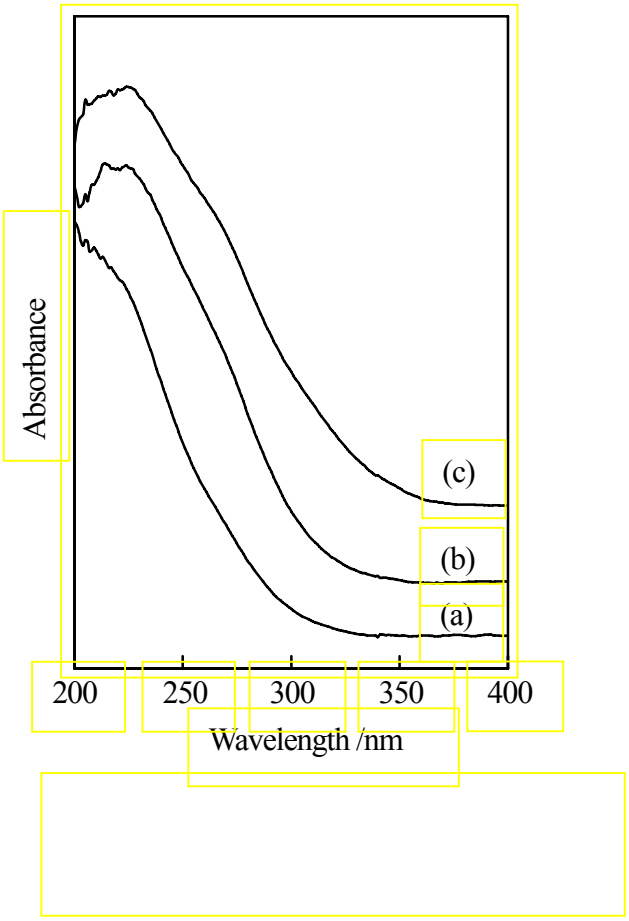

Figure 5. Y. Oumi et al.

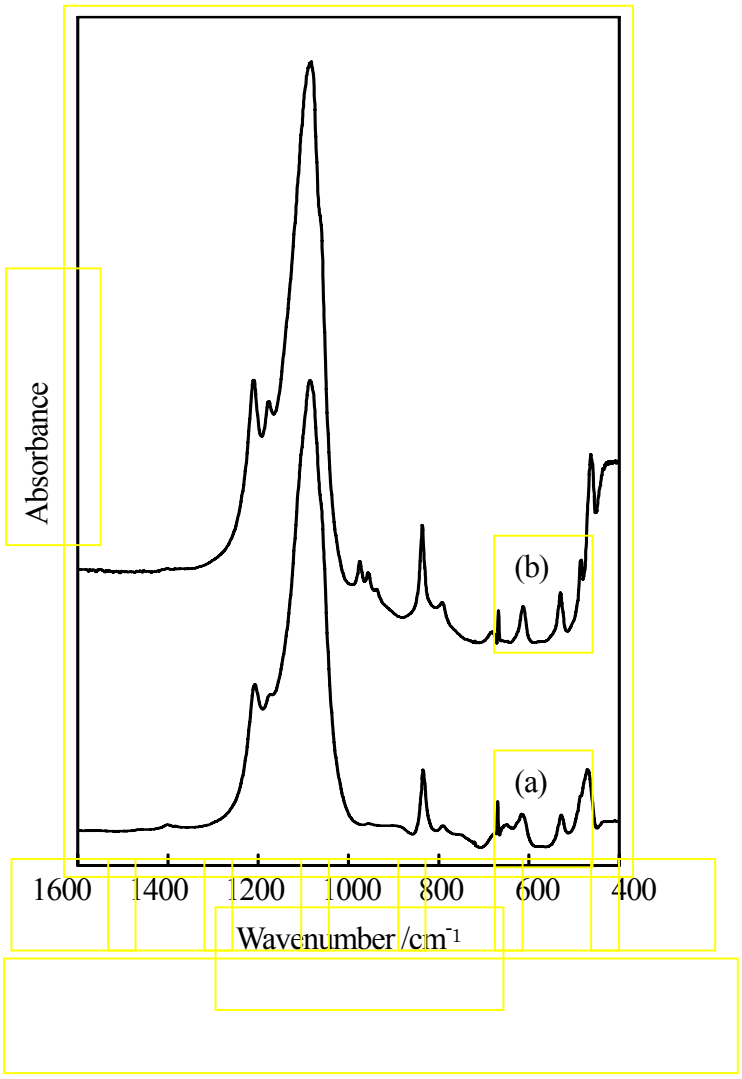

Figure 6. Y. Oumi et al.

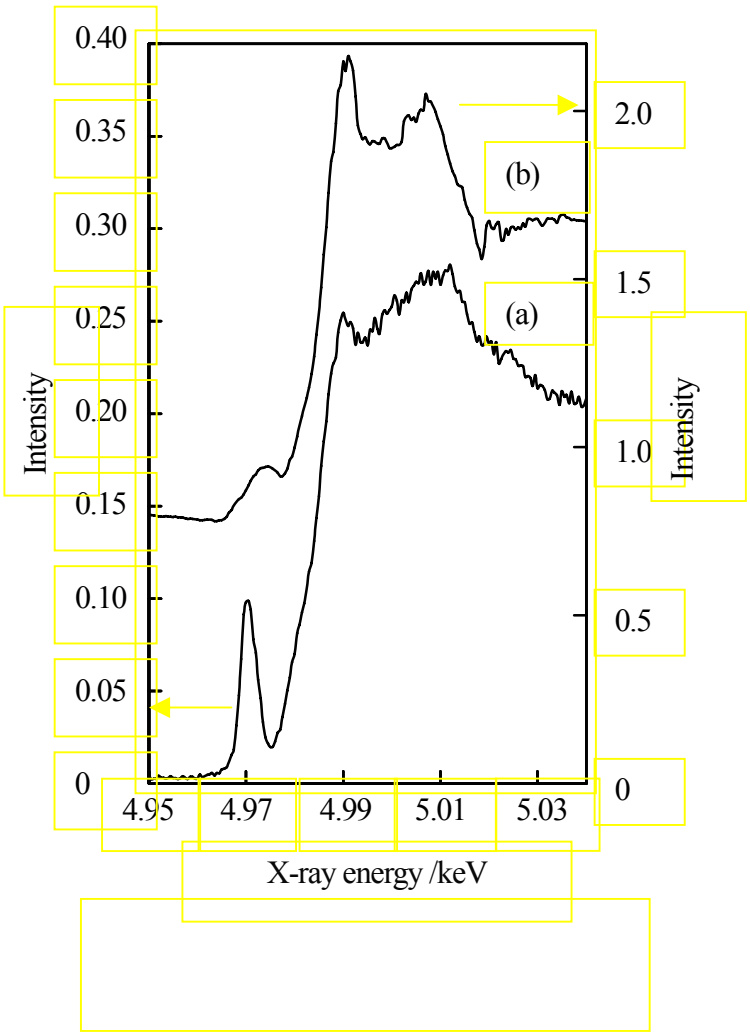

Figure 7. Y. Oumi et al.

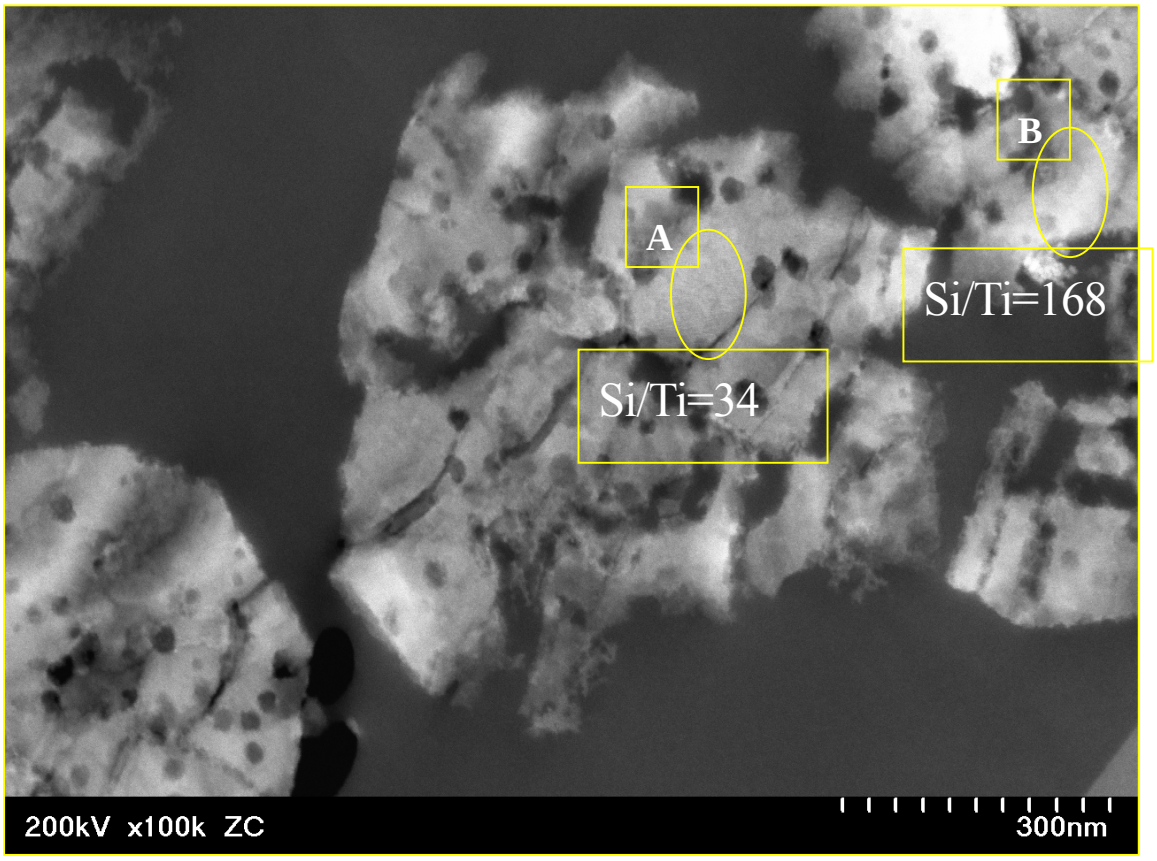

Figure 8. Y. Oumi et al.